

Article

Microstructure and Properties of Spot Welded Joints of Hot-Stamped Ultra-High Strength Steel Used for Automotive Body Structures

Zhixia Qiao ^{1,*}, Huijun Li ², Lianjin Li ³, Xiaoyu Ran ³ and Liwen Feng ³

¹ Tianjin Key Laboratory of Refrigeration Technology, Tianjin University of Commerce, Tianjin 300134, China

² School of Mechanical, Materials, Mechatronics and Biomedical Engineering, University of Wollongong, Northfields Avenue, Wollongong, NSW 2500, Australia; huijun@uow.edu.au

³ School of Mechanical Engineering, Tianjin University of Commerce, Tianjin 300134, China; lilianjin@163.com (L.L.); 13389905060@163.com (X.R.); fengliwen@163.com (L.F.)

* Correspondence: qzhxia@tjcu.edu.cn; Tel.: +86-1592-210-0905

Received: 1 February 2019; Accepted: 26 February 2019; Published: 2 March 2019



Abstract: Hot-stamped ultra-high strength steels have been widely used in automobile structural parts. Considering the high splash tendency in resistance spot welding due to their extremely high hardness, in this work, microstructural characteristics and mechanical performance of the resistance spot welded ultra-high strength steels are investigated. The results indicate that the interface between the nugget and heat-affected zone (HAZ) is the weakest zone where fractures initiate. In tensile shearing tests, a qualified spot welding joint failed with a button-shaped fracture. Welding defects would significantly decrease the load-carrying capacity and lead to interfacial fracture, except for a button-shaped fracture. In spot welding, it was found that a specific mid-frequency alternating current (AC) input mode, in which a 6 ms cooling cycle was inserted between every two neighboring current pulses, can avoid the splash in the spot welding of hot-stamped hardened steels.

Keywords: spot welding; hot-stamped hardened steel; microstructure; martensite; bainite

1. Introduction

Hot-stamped ultra-high strength steels have been widely used as automobile structural parts, due to the increasing requirements for safety and weight reduction of automobiles. The hot-stamped steel sheet is first heated to the austenite zone and then transferred quickly into deforming dies and hot pressed into structural components with required shapes, such as A-pillar, B-pillar, and bumpers, and finally is rapidly cooled to room temperature by flowing cooling water in dies. During the cooling process, essentially 100% martensite is produced, and the tensile strength can be up to 1500 MPa and the yield strength can reach 1100 MPa [1–3]. To avoid oxidation at high temperatures during hot stamping, the as-received steel sheets are usually pre-coated by Al-Si [4]. Resistance spot welding is one of the most important joining methods in automobile manufacture. However, the ultra-high strength steel exhibits a poor weld-ability during the spot welding process. Molten metal splash tends to occur in welding, which is related to the high hardness of the steel. On the one hand, the two overlapping steel sheets are hard to press together, and on the other, the contact resistance between the two ultra-high strength steel sheets is much higher than that of plain-carbon steels, which result in the faster melting of metal. Under the combined action of these two factors, splash is a common issue in the spot welding of ultra-high strength steel. Splash tends to cause many kinds of welding defects in the nugget and decreases the tensile capacity significantly. In order to optimize spot welding parameters of automobile steels, researchers have studied the influence of spot welding parameters, especially current, electrode force, and welding time, on the microstructure and mechanical properties

of spot welding joints [5–7]. In recent years, alternating current (AC) spot welding machines with variable frequency have been developed and more widely used in resistance spot welding in the automobile industry [8–10]. In this case, except for the above mentioned three traditional parameters, some other parameters like frequency and pulse duration would influence the spot welding process, and thereby the mechanical properties of the joints. However, studies have seldom considered the effect of austenite pre-strain, which results from electrode force during welding on the phase transformation of the heating affected zone (HAZ) after spot welding. In this work, the damage mechanism of spot welding joints of hot-stamped strengthened steels was studied in detail, and then spot welding experiments were performed with different current input modes in order to optimize the parameters of resistance spot welding and decrease the splashing ratio in welding.

2. Experiment

Boron bearing steel with an Al-Si coating was used in the present study (GMW14400M-ST-S-HS1300T/950Y-MS). Rectangular specimens for spot welding tests with a dimension of $100 \times 25 \times 1.5 \text{ mm}^3$ were cut from the hot-stamped hardened A-pillars or B-pillars. The chemical composition of the base steel was measured, and the results are shown in Table 1. The yield strength $R_{p0.2}$, tensile strength R_m , and elongation of the investigated hot-stamped hardened steel were determined as about 1100 MPa, 1500 MPa, and 5.4~7.7%, respectively. The microstructure of the hot-stamped hardened steel consists entirely of fine martensite, including martensite laths and plates, as shown in Figure 1. Microhardness of the hot-stamped hardened steel was determined as HV432.

Table 1. Chemical compositions of hot-stamped steel sheets (wt %).

C	Si	Mn	Cr	Ni	Mo	V	P	S	B	Fe
0.24	0.35	1.43	0.22	0.06	0.02	0.02	0.0317	0.0103	0.0025	base



Figure 1. Optical microstructure of the hot-stamped hardened steel.

In order to clarify the phase transformation of the experimental steel after experiencing reheating in spot welding, its continuous cooling transformation (CCT) diagram was obtained by dilatometry measurements. The steels were heated to 1000 °C at a heating rate of 100 °C/s for 2 min, and then cooled to room temperature with different cooling rates.

In resistance spot welding experiments, DC (direct-current) and variable frequency AC (alternating-current) power controllers (Sunke Co. LTD, Tianjin, China) were used in this study. Three types of current modes were applied: (1) DC, with current size of 8~9 kA and welding time of 300~350 ms; (2) general mid-frequency AC, with frequency of 110 Hz, current size of 10~11 kA, and welding time of 20 cycles; (3) mid-frequency AC with cooling intervals (about 6 ms) between any two neighboring current pulses, with frequency of 110 Hz, current size of 11~12.7 kA, and welding

time of 25~35 cycles. An electrode force of 550 kg was applied, and the diameter of the used electrode was 6 mm.

Specimens for microstructural examination were cut along a diameter of the spot welding nugget, as shown in Figure 2 by red dotted line of A-A. The specimen includes the whole cross section and it was embedded in epoxy resin with the cross section of the nugget at surface. One of the two cross sections was grounded and polished, and then etched with 3.5% nital reagent. Microstructural observations were conducted by optical microscopy (OM) (Leica DFC 450, Leica, Solms, Germany) and scanning electron microscopy (SEM) (Zeiss, Jena, Germany). Microhardness was determined to evaluate the property of different microstructural areas around the spot welding nuggets, by applying a load of 200 g. In order to examine the mechanical property of spot welding joints, tensile shear tests were performed using samples with dimensions as shown in Figure 2. Three samples were prepared for each welding condition and the average value of the three samples was used.

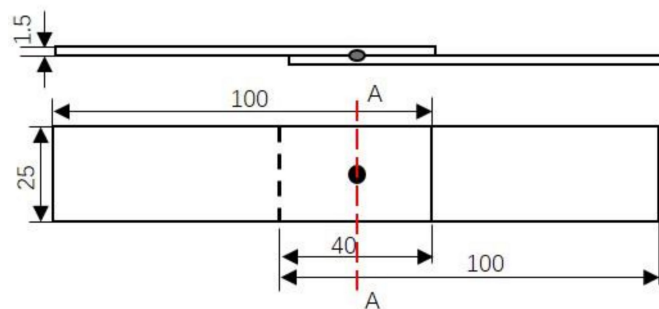


Figure 2. Specimen dimensions for tensile shear tests (unit: mm).

3. Results and Discussion

3.1. Continuous Cooling Phase Transformation

To elucidate the effect of the cooling rate on the phase transformation behavior of the experimental steel, the continuous cooling transformation diagram is established, as shown in Figure 3. Figure 4 shows the microstructures under different cooling rates. It can be seen that the critical cooling rate for martensite transformation was close to 17 °C/s, in which the microstructure consisted entirely of martensite, indicating the high hardenability of the steel. Under the slow cooling rate of 1.5 °C/s, as shown in Figure 4a, the microstructure consisted of polygonal ferrite and a small amount of pearlite, which was formed in the range 603~678 °C, as seen from Figure 3. With the cooling rate increasing to 3 °C/s, polygonal ferrite transformed to an acicular one, and a small amount of granular bainite could be found, as indicated by arrows in Figure 4b. The acicular ferrite nucleates at prior austenite grain boundaries and grows into the prior austenite grains. In the case of 3 °C/s, the phase transformation occurred in the temperature range 556~620 °C, as seen from Figure 3. As the cooling rate further increased to 8 °C/s, granular bainite tended to predominate in the produced microstructure, as shown in Figure 4c. As the cooling rate went higher than 17 °C/s, the product was completely martensite, as shown in Figure 4c. The martensite start and finish temperatures (M_s and M_f) were respectively determined as 438 and 339 °C.

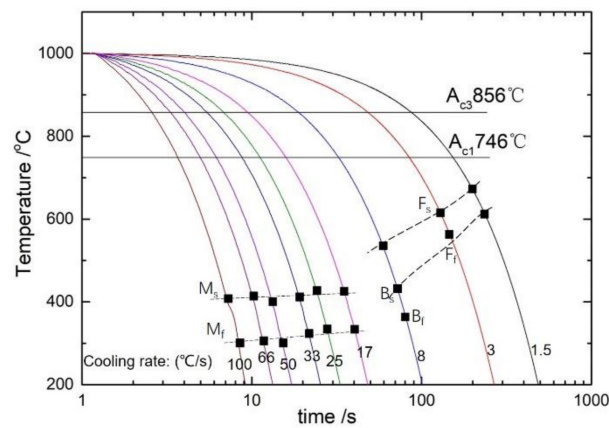


Figure 3. Continuous cooling transformation diagram of the experimental hot stamping steel.

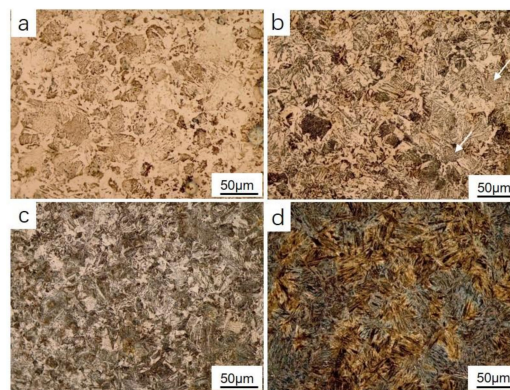


Figure 4. Optical microstructures under typical cooling rates: (a) 1.5 °C/s, (b) 3 °C/s, (c) 8 °C/s, (d) 17 °C/s.

3.2. Microstructures of a Spot Welded Joint

Figure 5 shows the low-magnification microstructure of a whole spot welding joint, which was obtained under mid-frequency AC with cooling intervals of 6 ms between any two neighboring current pulses (named AC-6), with a peak current of 12 kA, frequency of 110 Hz, and welding time of 35 cycles. In Figure 5, a whole nugget with a diameter of about 6 mm can be clearly seen, as shown by the yellow double-headed arrow. It is known that $4\sqrt{t}$ (t denotes sheet thickness) is the minimum requirement for the nugget diameter. Thickness of the sheet samples used in this work was 1.5 mm, and thus the $4\sqrt{t}$ should be 4.9 mm. The actually obtained diameter was much larger than the standard requirement for a spot welding nugget.

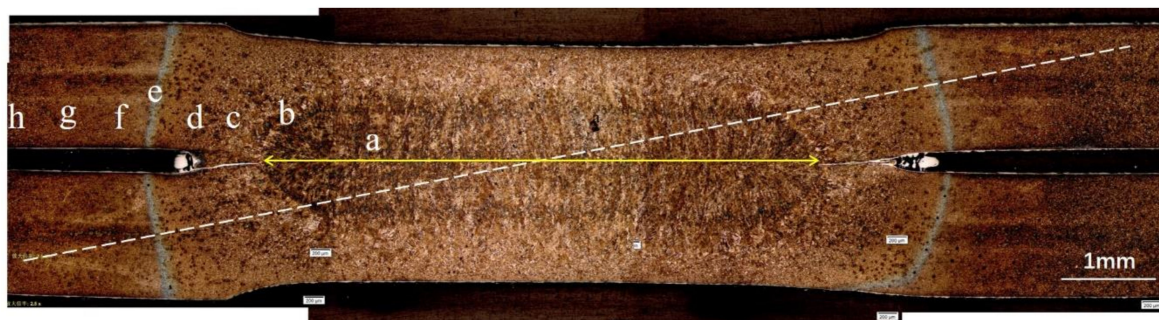


Figure 5. Low-magnification optical microstructure of a whole spot welding joint obtained at AC-6, with a peak current of 12 kA, frequency of 110 Hz, and welding time of 35 cycles.

The spot welded joint includes three regions: nugget, heat-affected zone (HAZ), and base metal. There were two micro areas, just like two white arc lines, on the left and right sides of the nugget in each steel sheet, just outside the upper and under indentations, marked by “e” in Figure 5. These areas exhibited as white due to the specific microstructure of acicular ferrite. Figure 6 presents the microstructures of different regions in Figure 5. The nugget was formed by solidification of melted base metal after spot welding, and it consisted of a columnar grain perpendicular to the surface of steel sheets. Due to the strong cooling effect resulting from the flowing water inside Cu electrodes, the nugget after spot welding was cooled at a rate much higher than the critical quenching rate, and its microstructure was completely composed of martensite, as shown in Figure 6a. Although the martensitic transformation in the nugget occurred within the large columnar austenite grains, martensite laths were relatively fine and dense. The widths of the columnar austenite grains were generally small and less than 50 μm , and most martensite laths form by crossing the width of the columnar grains, therefore, the lengths of the martensite laths were limited within the widths of the columnar austenite grains and were exhibited as fine and dense.

At the interface between the nugget and HAZ, i.e., the fusion zone, extremely coarse prior austenite grains can be distinguished, as shown in the lower right part of Figure 6b. The large-sized austenite grains were related to the higher austenitizing temperature, which was close to the melting point of the steel. This region would be the weakest part of the whole spot welding joint upon loading.

Just outside the fusion zone, the microstructure consisted of relatively fine martensite, as shown on the upper left part of Figure 6b. With the distance away from the nugget center increasing, the maximum heating temperature in welding was decreased, and the size of martensite laths was decreased, as shown in Figure 6c,d. From the fusion zone to the white arc line (marked by “e” in Figure 5), the microstructure was just composed of martensite.

Figure 6e and 6e' show the OM and SEM images of the microstructure in the white arc line in Figure 5. The microstructure in this area consisted of fine acicular ferrite. The width of the white arc line region was about 100 μm and it was a part of the HAZ of a spot welding joint. This region is suggested to be completely austenitized during the welding process, but the cooling rate was too slow to obtain the martensite, since it was relatively far away from the electrodes and cannot be effectively cooled by the flowing water inside the electrodes. It should be noted that the acicular ferrite in Figure 6e is much finer than that in Figure 4b. It was reported that the pre-strain imposed on austenite could affect the phase transformation behavior in subsequent cooling process [11]. Pre-strain can produce a considerable amount of crystal defects (dislocations) within austenite grains. These defects can serve as nuclei for ferrite, therefore ferrite can not only nucleate on grain boundaries but also within the austenite grains. Abundant nucleation sites within austenite grains result in the formation of fine acicular ferrite. When the pre-strain is absent, ferrite would nucleate only on grain boundaries and grow into the austenite grain, resulting in the formation of coarse acicular ferrite, as shown in Figure 4b. From Figure 5, the white arc lines were located just outside the electrode indentation, where the pre-strain accumulated significantly in prior austenite grains. Coupled with the lowest cooling rate, fine acicular ferrite was produced in this region. This area also exhibited the lowest hardness in the whole spot welding joint.

Regions outside the white arc line areas experienced a faster cooling rate due to better heat conduction into surrounding material, and the microstructures were composed of granular bainite, as shown in Figure 6f,g. In addition, with the distance away from the nugget increasing, the density of particles in granular bainite increased and the polygonal bainite matrix evolved to a lath-shaped one. Figure 6h shows the microstructure far away from the nugget, where the peak heating temperature was lower than A_{c1} and the martensite in base metal was tempered to some extent.

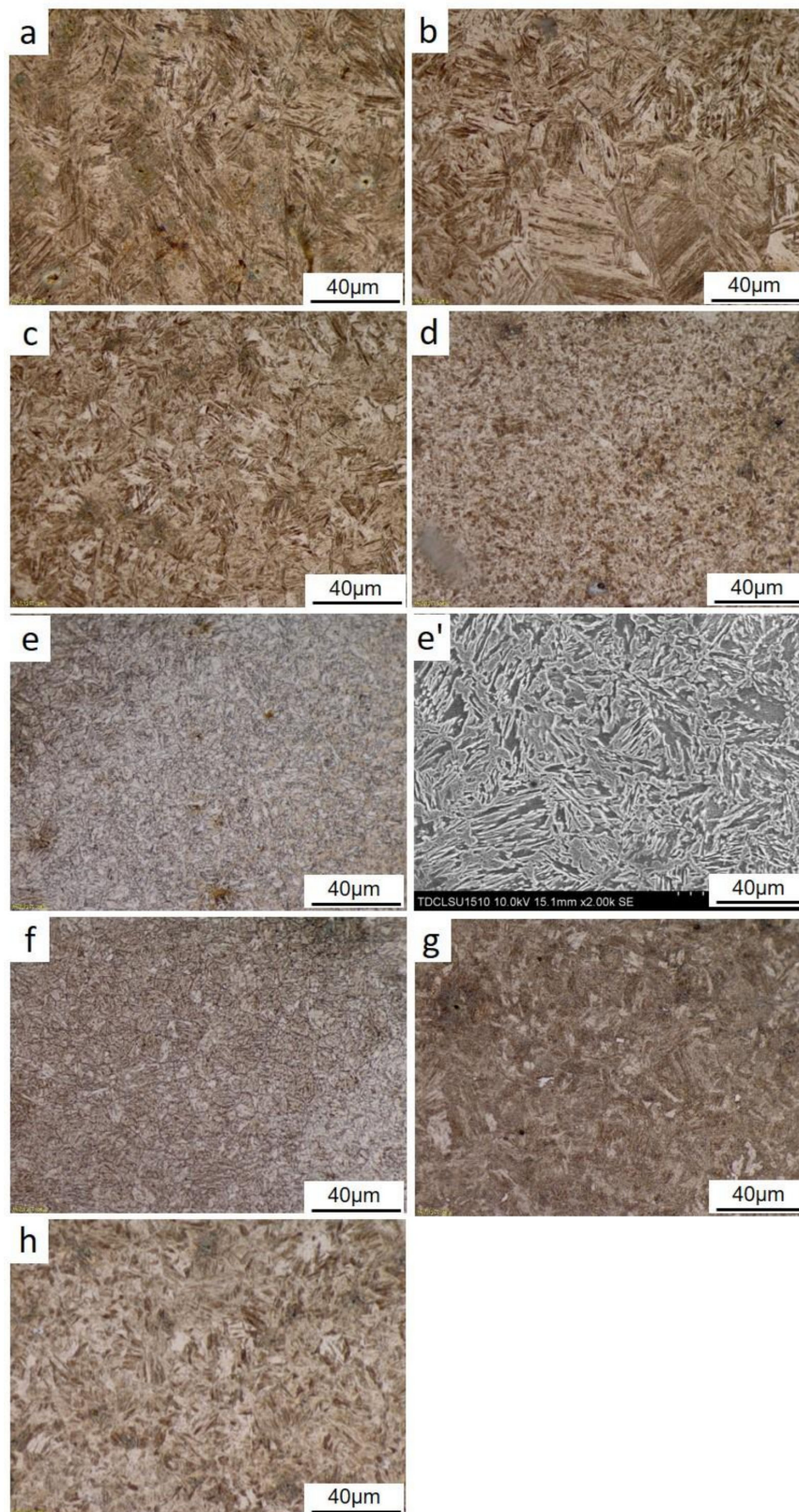


Figure 6. Microstructures of different micro regions in a spot welding joint, corresponding to (a)~(e) marked in Figure 5: (a) nugget, composed of fine martensite within columnar grains; (b) fusion zone, mix of coarse martensite and fine martensite; (c) martensite; (d) minute martensite; (e) acicular ferrite under an optical microscope; (e') acicular ferrite under SEM; (f) granular bainite with polygonal matrix; (g) granular bainite with a lath-shaped matrix; (h) tempered martensite.

3.3. Micro-Hardness Distribution Across a Spot Welded Joint

Figure 7 shows the distribution of hardness along the white dashed line in Figure 5. The microhardness of the nugget is somewhat higher than that of the base metal, by about 30–50 HV. This resulted from the extra-high cooling effect of the electrodes on the phase transformation. The region just outside the nugget, which consisted of martensite, had a hardness slightly lower than that of the nugget. The lowest hardness throughout the welding joint in Figure 7 (about 310 HV) corresponds to the white arc line regions in Figure 5, which consist of acicular ferrite. Outward from the white arc line regions, the cooling rate increased rapidly and granular bainite was obtained, therefore, microhardness rose sharply. Microhardness tended to stabilize at about 450 HV as soon as the base metal appeared.

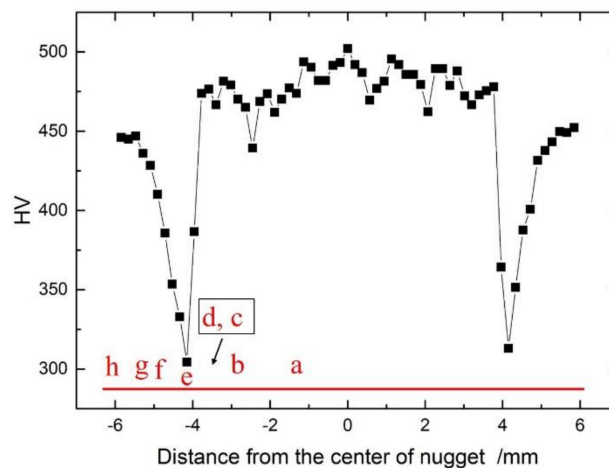


Figure 7. Microhardness measurement results on the typical spot welded joint in Figure 5; (a)–(h) correspond to the micro areas in Figure 5.

3.4. Tensile Shear Fracture

Spot welding joints exhibit two types of fracture modes: button-shaped fractures and interfacial fractures. A spot welded joint is generally considered to be qualified if a button-shaped fracture is produced when the applied load exceeds its capacity in tensile shearing tests. That is, the whole joint is integrally pulled away from one of the two overlapped sheets, leaving a hole in this sheet and a button on the other one. Figure 8 is an overall view of a failed specimen as a button fracture, obtained at AC-6, with a peak current of 12.7 kA, frequency of 110 Hz, and welding time of 35 cycles. In tensile shear tests, in order to discover the origin of cracks, a high-speed camera was used to take continuous photographs of the weld surface during loading. It was learned from the obtained continuous pictures that for any one of the two overlapped sheets, stresses concentrate significantly on the chuck-nearing side of the joint at an early loading stage, as shown by the two rectangles in Figure 8a. For the upper sheet in Figure 8a, stress concentrates at the right side of the joint and for the lower sheets, stress concentrates at the left side. When stress exceeds the strength of the joint, cracks originate at these stress concentration sites and subsequently fracture occurs. Once cracks appear on either side, the stress concentration on the other side would be relieved greatly, and afterwards the cracks further develop until fracture takes place at that side. From the low-magnification optical micrograph shown in Figure 8b, it is known that fracture originated on the boundary of the nugget, i.e., the fusion zone, which consisted of coarse martensite, as shown in Figure 6b. This indicates that the fusion zone is the weakest region throughout the weld joint, although the white arc line region is the softest region, consisting of acicular ferrite. Figure 8c shows a magnified SEM image of the fracture edge, clearly showing that the original fracture occurred on the boundaries of coarse grains. Later, tearing occurred along half of the nugget edge on the fractured sheet and the nugget was left on the other sheet, leaving a button. Under large compressive stress, the opposite side of the fracture

originating point in the joint was deformed significantly, and the formed fiber-like structure is marked by white arrows in Figure 8d.

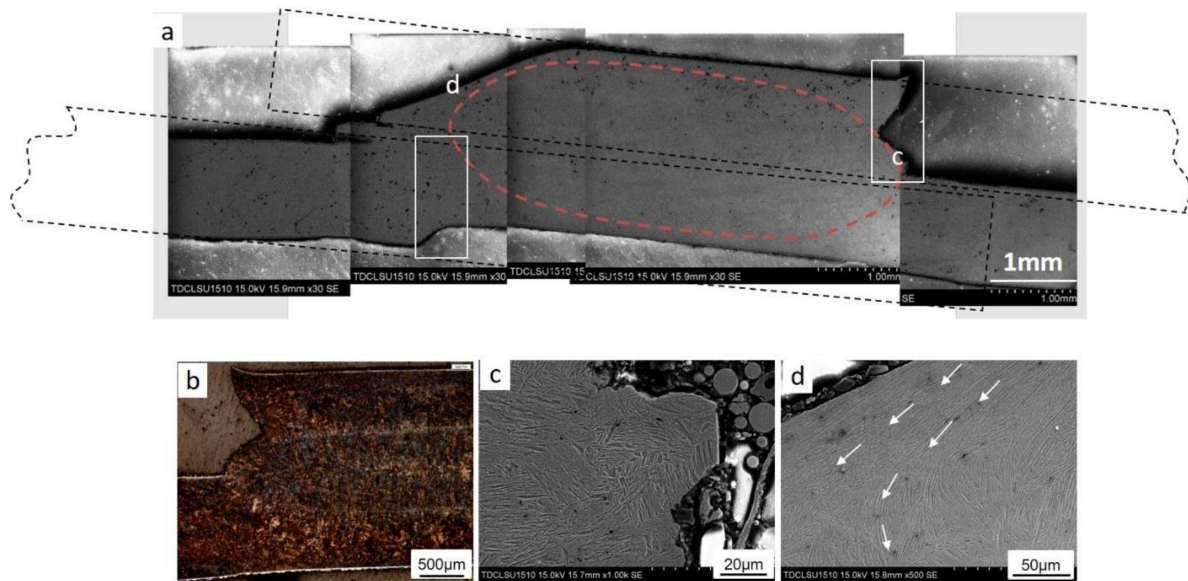


Figure 8. Button-shape fracture images, obtained at AC-6, with a peak current of 12.7 kA, frequency of 110 Hz, and welding time of 35 cycles: (a) overall view of a fractured joint, (b) optical image showing nugget, (c) SEM image of fracture edge at “c” point, (d) SEM image of fracture edge at “d” point.

A spot welding joint with the interfacial fracture mode is generally considered unqualified. In this case, the nugget was divided into two parts along the bonding surface of two overlapped sheets. The flat fracture surface is left on each sheet. In this case, the spot welding joint fails mainly under the action of shearing force. Figure 9 shows the typical morphology of an interfacial fracture surface in a failed specimen in tensile shear tests. It can be noted that many small cracks exist in the nugget, as shown in Figure 9a. Such small cracks tend to form in the spot welding process when splash occurred, in which shrinkage stresses were more likely to be produced. High-magnification observation on regions around the cracks shows no dimple produced after fracture, as marked by white circles in Figure 9b, indicating that brittle fracture occurred around cracks. Yet regions far away from the cracks exhibit plastic fracture characteristics, with a lot of dimples left. Some areas exhibit typical shearing fracture characteristics, with small dimples stretched along a uniform direction, as shown in Figure 9c,d, indicating that shearing stress was responsible for the fracture. In addition, inclusions and shrinkage defects in the nugget were also factors leading to interfacial fracture, because their appearance would decrease the effective loading area of the joint.

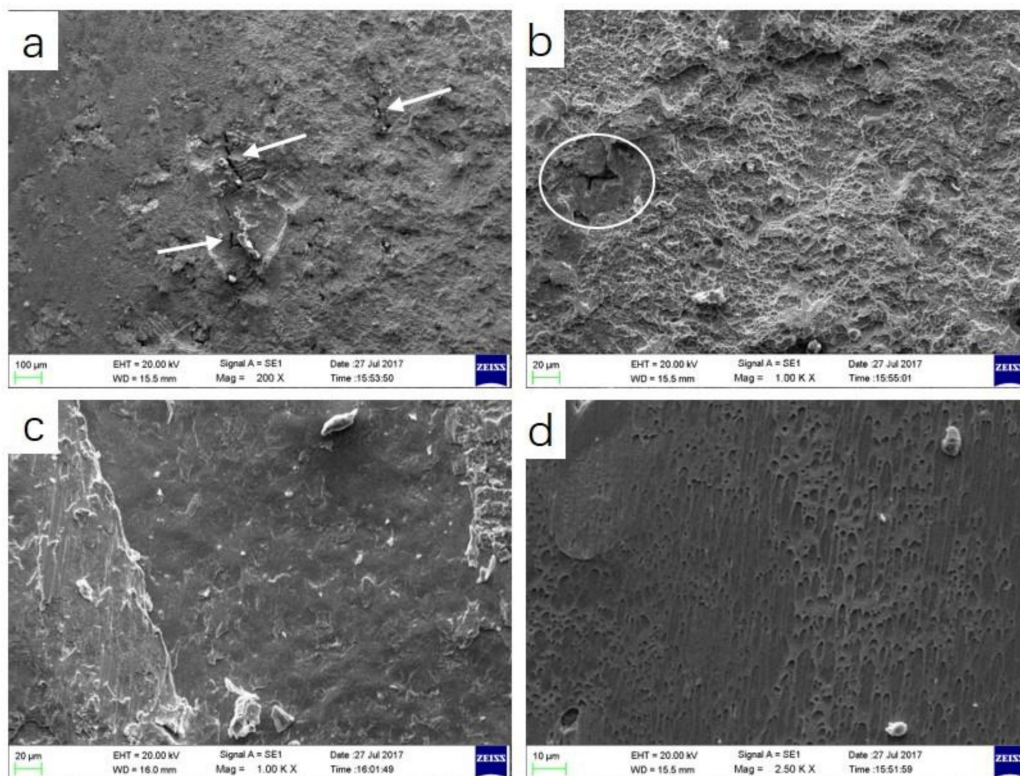


Figure 9. SEM images of an interfacial fractured specimen: (a) showing small cracks at low magnification, (b) showing brittle fracture around cracks and plastic fracture far away from cracks, (c) shearing surface, (d) stretched dimples on shearing surface.

3.5. Parameter Optimization for Spot Welding of Hot-Stamped Hardened Steels

In case of spot welding of hot-stamped hardened steel, splash is an important problem demanding a solution. This is due to its ultra-high hardness, which requires a relatively large electrode force to keep the two overlapped sheets in close contact. Therefore, liquid metal tends more to be squeezed out from the molten nugget and thus splash occurs. In this case, a larger plastic metal ring around the molten nugget is beneficial for avoiding splash in spot welding. In order to optimize the technology of spot welding of hot-stamped hardened steel, three current modes were used in this investigation—direct current (DC), mid-frequency alternative current (AC), mid-frequency AC with a 6 ms cooling interval every other cycle (named AC-6)—as shown in Figure 10.

For the AC-6, the time interval was inserted between two neighboring cycles aiming to slow down the expanding rate of the molten metal nugget, and at the same time give more time for the plastic ring areas to expand outward. This is beneficial for the molten metal to be included in the plastic ring and prevent splash happening. Large enough plastic ring areas are important for avoiding splash in spot welding, which can ensure the molten metal is enclosed through close contact of the two overlapped sheets at the plastic areas under great pressure from electrode forces. The length of the time interval should be long enough to ensure the plastic ring expands faster than the molten metal nugget. If the length of the interval is too long, the nugget size would be too small and more welding time would be needed for a joint. After experimenting repeatedly, 6 ms was determined for the experimental ultra-high strength steel of 1.5 mm thickness.

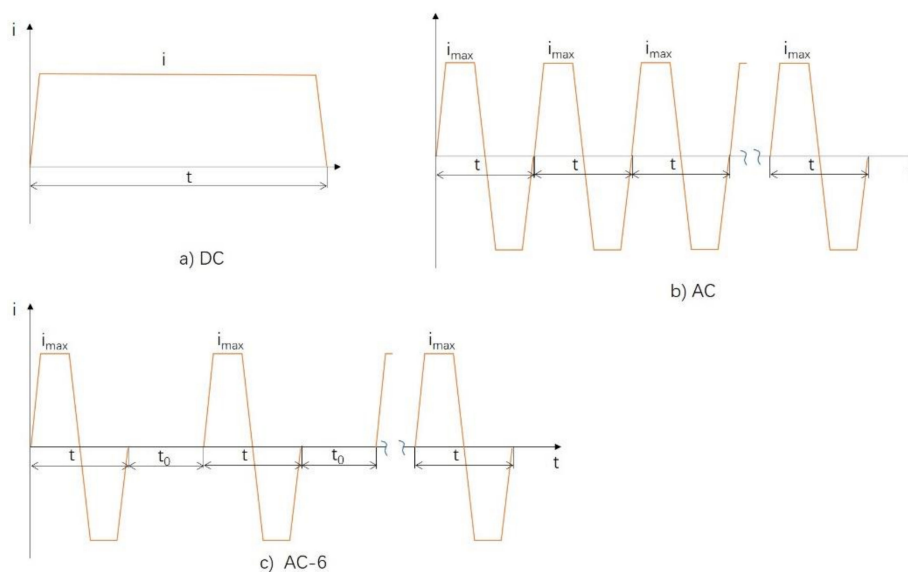


Figure 10. Current modes applied in the present investigation: (a) DC: direct current, (b) AC: mid-frequency alternating current, (c) AC-6: mid-frequency alternating current with a 6 ms cooling interval every other cycle.

Under the two spot welding conditions of AC (AC and AC-6), it was found that the frequency of 110 Hz was the most suitable parameter for the present steel through a series of orthogonal tests by changing current value and frequency. Therefore, frequency of 110 Hz was used here. Under each welding condition, the most suitable current was determined and used, as shown in Table 2. Spot welding test results are summarized in Table 2, showing the diameter of the nugget, splash ratio, and maximum bearable tensile load. It was AC-6 that can solve perfectly the splash problem in spot welding, and only 5% of weld joints were splashed.

Table 2. Spot welding test results using three different current modes.

Current Mode	i_{max}/kA	Virtual Current/kA	Weld Time/ms	Nugget Diameter/mm	Non-Splash Ratio	Max-Tensile Load/kN
AC-6	11	6.8	377	6.2	95%	22
AC	11	9.49	182	5.5	10%	19
DC	8.5	8.5	300	5.7	10%	13.5

It is known that a plastic metal ring around the nugget is important for avoiding splash during spot welding, which can encircle the molten nugget and prevent it from splashing out. Therefore, keeping a large enough plastic ring during welding is important for avoiding splash. At the end of heating, the liquid molten nugget has the largest volume, and at the same time, the surrounding metal is in austenite condition and exhibits good ductility. Under the large electrode force, the austenite zone is extruded significantly, leading to the two overlapped sheets compressed against each other closely. Therefore, the HAZ with a large width is more favorable in order to avoid splash in spot welding. The distance from edge of the nugget to the nearest white arc line was measured for the three welding conditions using different current modes, as shown in Figure 11. The results, as shown in Figure 11d, indicate that the distance from edge of the nugget to the nearest white arc line is the largest under the AC-6 condition, which proves that the austenite zone around the nugget plays an important role in avoiding splash.

From Table 2, it is noted that the welded joints obtained under the AC-6 condition exhibit the highest mechanical property (maximum tensile load). In tensile shearing tests, the welded joints under AC-6 always fractured with a button-shaped mode, yet interfacial fractures may occur in samples

obtained under AC and DC conditions. Microstructural examination of the welded joints obtained under three different current modes was carried out. Defects like shrinkage holes, micro cracks, and Al-Si inclusions were found in DC and AC specimens, as shown in Figure 12a–d. These defects probably result from the splash during the welding process. Splash leads to the reduction of liquid metal in the nugget, resulting in the solidification shrinkage holes and cracks. In addition, some molten Al-Si coating was pushed back into the liquid nugget when splash occurred and led to Al-Si inclusions in the nugget, as shown in Figure 12a,c, which significantly decreases the load-carrying capacity of the spot welding joint. Microstructural examinations on the spot welding joint of the AC-6 specimen showed that the microstructure in the nugget was in good condition, and there were no obvious weld defects.

It can be concluded from the above results that applying AC with 6 ms intervals between two neighboring cycles is a good method to address the splash problem in spot welding of hot-stamped hardened steels, and thus increase evidently the tensile shearing property.

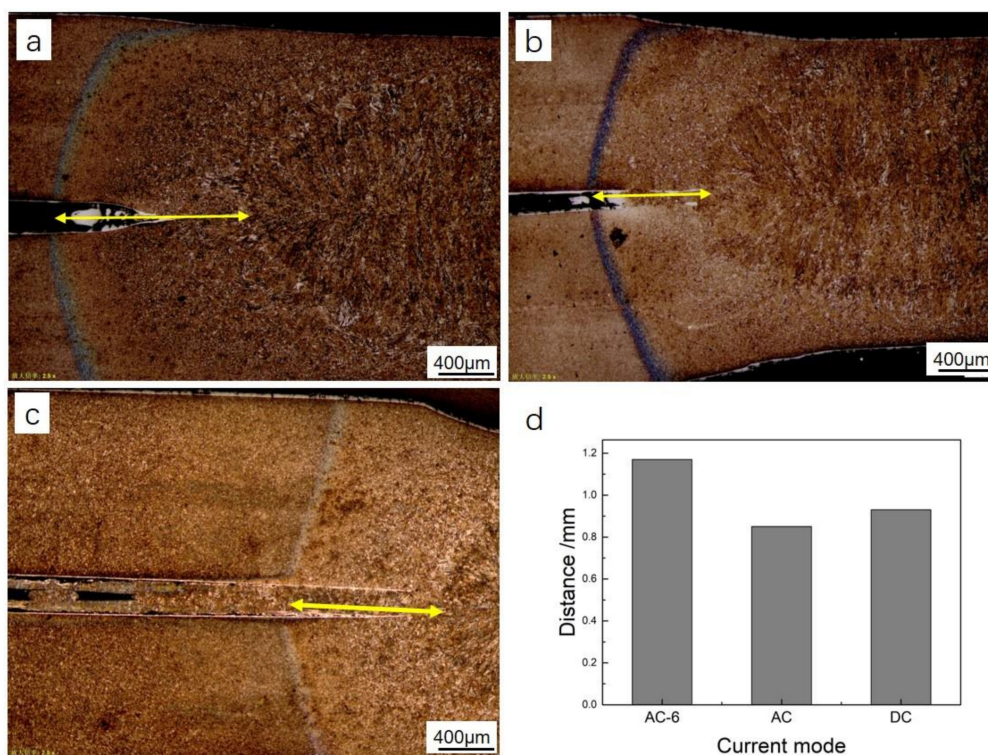


Figure 11. Comparison of plastic zone size under three conditions with different current modes: (a) AC-6, (b) AC, (c) DC, (d) results summarization.

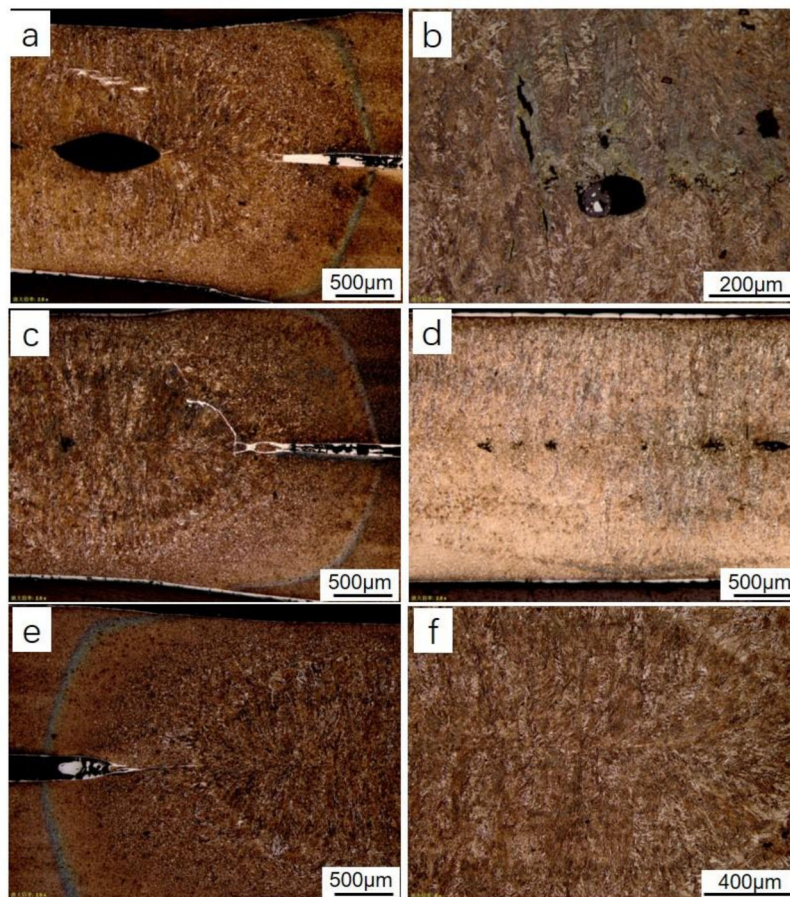


Figure 12. Various defects produced in spot welded specimens applying AC and DC, showing shrinkage holes, Al-Si inclusions, and cracks: (a) and (b) AC condition, (c) and (d) DC condition, (e) and (f) AC-6 condition.

4. Conclusions

The microstructure of spot welded joints of hot-stamped hardened steel was studied by establishing a CCT diagram and microstructural examination. Nugget microstructure completely consisted of martensite within columnar crystals and HAZ was composed of coarse martensite, fine martensite, acicular ferrite, granular bainite, and tempered martensite, in the order from nugget edge to outside. The nugget exhibited the highest microhardness and the acicular ferrite zone was the softest area.

The boundary between the nugget and the coarse martensite zone was the weakest area and fracture was prone to occur in the boundary when the tensile shearing load exceeded its limit. Therefore, for a qualified spot welding joint, a button-shape fracture was generally obtained. If a joint has a lot of welding defects, i.e., shrinkage holes, cracks, and Al-Si inclusions, interfacial fracture tends to occur, which is characterized by a shearing fracture.

Splash is liable to produce various defects in a spot welded nugget, resulting in interfacial fracture of the joint. The splash problem in the spot welding of hot-stamped hardened steel was solved perfectly by using a specific mid-frequency AC current input mode, in which a 6 ms cooling cycle was inserted between every two neighboring current pulses. Under traditional mid-frequency AC and DC heat input modes, splash easily occurs in spot welded joints, resulting in defects in the nugget, and significantly decreasing the load-carrying capacity of welded joints.

Author Contributions: Writing—original draft preparation, Z.Q. and H.L.; investigation, L.L.; formal analysis, X.R. and L.F.

Funding: This research was funded by the Key Technologies R & D Program of Tianjin (Grant No. 18YFZCGX00050), the National Natural Science Foundation of China (Grant No. 51204121), and the Natural Science Foundation of Tianjin City (Grant No. 16JCTPJC48900).

Conflicts of Interest: The authors declare no conflict of interest.

References

1. Merklein, M.; Wieland, M.; Lechner, M.; Bruschi, S.; Ghiotti, A. Hot stamping of boron steel sheets with tailored properties: A review. *J. Mater. Process. Technol.* **2016**, *228*, 11–24. [[CrossRef](#)]
2. Karbasian, H.; Tekkaya, A.E. A review on hot stamping. *J. Mater. Process. Technol.* **2010**, *210*, 2103–2118. [[CrossRef](#)]
3. Yi, H.L.; Ghosh, S.; Bhadeshia, H.K.D.H. Dual-phase hot-press forming alloy. *Mater. Sci. Eng. A* **2010**, *527*, 4870–4874. [[CrossRef](#)]
4. Ighodaro, O.L.; Biro, E.; Zhou, Y.N. Comparative effects of Al-Si and galvanized coatings on the properties of resistance spot welded hot stamping steel joints. *J. Mater. Process. Technol.* **2016**, *236*, 64–72. [[CrossRef](#)]
5. Jong, Y.-S.; Lee, Y.-K.; Kim, D.-C.; Kang, M.-J.; Hwang, I.-S.; Lee, W.-B. Microstructural Evolution and Mechanical Properties of Resistance Spot Welded Ultra High Strength Steel Containing Boron. *Mater. Trans.* **2011**, *52*, 1330–1333. [[CrossRef](#)]
6. Choi, H.-S.; Park, G.-H.; Lim, W.-S.; Kim, B.-M. Evaluation of weldability for resistance spot welded single-lap joint between GA780DP and hot-stamped 22MnB5 steel sheets. *J. Mech. Sci. Technol.* **2011**, *25*, 1543. [[CrossRef](#)]
7. Lu, Y.; Peer, A.; Abke, T.; Kimchi, M.; Zhang, W. Subcritical heat affected zone softening in hot-stamped boron steel during resistance spot welding. *Mater. Des.* **2018**, *155*, 170–184. [[CrossRef](#)]
8. Ding, L.; Min, H. Simulink and design of mid-frequency inverter resistance spot welding control system. *Electr. Weld. Mach.* **2015**, *45*, 26–31.
9. Brezovnik, R.; Cernelic, J.; Petrun, M.; Dolinar, D.; Ritonja, J. Impact of the switching frequency on the welding current of a spot-welding system. *IEEE Trans. Ind. Electron.* **2017**, *64*, 9291–9301. [[CrossRef](#)]
10. Son, J.-I.; Im, Y.-D. Intelligent Controller Implementation for Decreasing Splash in Inverter Spot Welding. *IEICE* **2009**, *92*, 1708–1712. [[CrossRef](#)]
11. Yogo, Y.; Kurato, N.; Iwata, N. Investigation of Hardness Change for Spot Welded Tailored Blank in Hot Stamping Using CCT and Deformation-CCT Diagrams. *Metall. Mater. Trans. A* **2018**, *49*, 2293–2301. [[CrossRef](#)]



© 2019 by the authors. Licensee MDPI, Basel, Switzerland. This article is an open access article distributed under the terms and conditions of the Creative Commons Attribution (CC BY) license (<http://creativecommons.org/licenses/by/4.0/>).